International Journal of Physics and Mathematics

E-ISSN: 2664-8644
P-ISSN: 2664-8636
IJPM 2025; 7(1): 170-180

www.physicsjournal.net
Received: 14-03-2025
Accepted: 16-04-2025

Nalini S Patil
Department of Mathematics, Pratap College, Amalner, Maharashtra, India

Ekta A Dixit
Department of Mathematics, Veer Narmad South Gujarat University, Surat, Gujarat, India

Corresponding Author:
Nalini S Patil
Department of Mathematics, Pratap College, Amalner, Maharashtra, India

A symmetrical study of heat and mass transfer in Prandtl fluids: Radiative, reactive, and resistive interactions

Nalini S Patil and Ekta A Dixit

DOI: https://www.doi.org/10.33545/26648636.2025.v7.i1b.132

Abstract
The present study investigates the complex dynamics of heat and mass transfer in Prandtl fluids affected by the combined effects of thermal radiation, chemical reactions, and resistive (Joule) heating. This flow setup is crucial in many engineering and industrial applications, including high-temperature polymer processing, chemical manufacturing, and energy systems where thermal and reactive transport processes coexist. A two-dimensional, steady, incompressible flow model is created to describe the behavior of a non-Newtonian Prandtl fluid flowing over a stretching surface. The governing partial differential equations, which include momentum, energy, and concentration transport, are converted into a system of nonlinear ordinary differential equations using suitable similarity transformations. These equations are then solved numerically with a fourth-order Runge-Kutta method combined with a shooting technique to accurately meet the boundary conditions. The effects of key parameters, such as the radiation parameter, Prandtl number, Schmidt number, chemical reaction rate, and Joule heating coefficient, are thoroughly analyzed. Results show that thermal radiation notably increases the fluid temperature, thereby thickening the thermal boundary layer. Chemical reactions have a dual influence: for generative reactions, concentration profiles rise, while for destructive reactions, species concentration decreases. Joule heating adds to the system's overall energy, enhancing thermal diffusion and raising both the temperature and velocity of the fluid.

Keywords: Prandtl fluid, dufour-soret effect, magnetohydrodynamics (MHD), and resistive heating

1. Introduction
In industrial processes such as metallurgical operations, nuclear reactor cooling, and magnetic drug targeting, magnetohydrodynamics-which studies the behavior of electrically conducting fluids in the presence of magnetic fields-is essential. Including magnetic fields in fluid flow introduces Lorentz forces, which can either suppress or enhance fluid motion, depending on the magnetic field's orientation and strength. For example, in nuclear fusion reactors, MHD is used to control plasma flows, improving reactor stability. In biomedical applications, magnetic nanoparticles are directed by external magnetic fields for targeted medication delivery. In the case of Prandtl fluids, MHD effects are vital for understanding flow stability, controlling thermal gradients, and optimizing heat transfer. The interaction between MHD and nanofluids creates unique phenomena resulting from the interplay of magnetic fields and nanoparticles, affecting both momentum and energy transport. Applications of MHD are found in fields such as nuclear reactors, MHD accelerators, power generation, and biomedical sensors [1,2]. Using a Lie group approach, Rajput *et al.* [3] studied MHD mixed unsteady flow over a vertical porous sheet. Amanulla *et al.* [4] analyzed the steady MHD flow of Prandtl fluids beyond a permeable sphere. The Hussain group [5] investigated the flow of Prandtl-Eyring fluid over a stretched surface in the presence of a magnetic field.
The effects of heat radiation and chemical reactions on the peristaltic flow of Prandtl fluid were examined by Hayat *et al.* [6]. Rajesh and Rajasekhara [7] described MHD Prandtl fluid through a tapered tube with heat radiation. Patil *et al.* [8] studied an unstable MHD Powell-Eyring nanofluid over a stretched sheet subjected to radiation and convective heating. In [9-13], additional research on the effects of heat radiation on non-Newtonian fluid flow was published. Numerous scientific and technical applications, such as energy conversion, chemical manufacture, and environmental systems, depend on heat and mass transfer processes. The thermal conductivity of Prandtl nanofluids is dramatically changed by the

addition of nanoparticles, which results in improved heat dissipation. Diffusion and interactions between nanoparticles and the base fluid affect mass transfer rates in nanofluids. The MHD Prandtl fluid's peristaltic flow in a double-diffusion rotating tube was examined by Hayat *et al.* [14]. A study of double diffusion flow on a stretched cylinder by Batool *et al.* [15] found a negative correlation in between the Prandtl number and temperature profile. The latest studies have looked at double diffusion effects [16-18]. In engineering applications such as geothermal energy extraction, considering viscous dissipation is essential for accurate thermal performance predictions. Mishra *et al.* [19] investigated several slip effects on MHD nanofluids and ohmic heating with velocity. A recent study by Jawad *et al.* [20] examined how MHD influences bioconvective nanofluids. Reports on current studies of viscous dissipation and Joule heating are available [21-24]. Following a review of the recent literature, studies of Prandtl fluid boundary layer flow under physical constraints like magnetic fields and thermal radiation are discussed. The system of partial differential equations (PDEs) is reformulated using similarity invariants and guided by the physical flow with appropriate boundary conditions. Graphical representations of non-dimensional physical properties are used to analyze the flow limitations revealed.

Mathematical Formation

An unstable, incompressible Prandtl fluid flow across a permeable stretched sheet was taken into consideration. The stretching sheet is parallel to x-axis, while the y-axis is perpendicular to it. Figure 1 illustrates how the surface is subjected to the magnetic flux $B = B_0\, x^{-1/2}$.

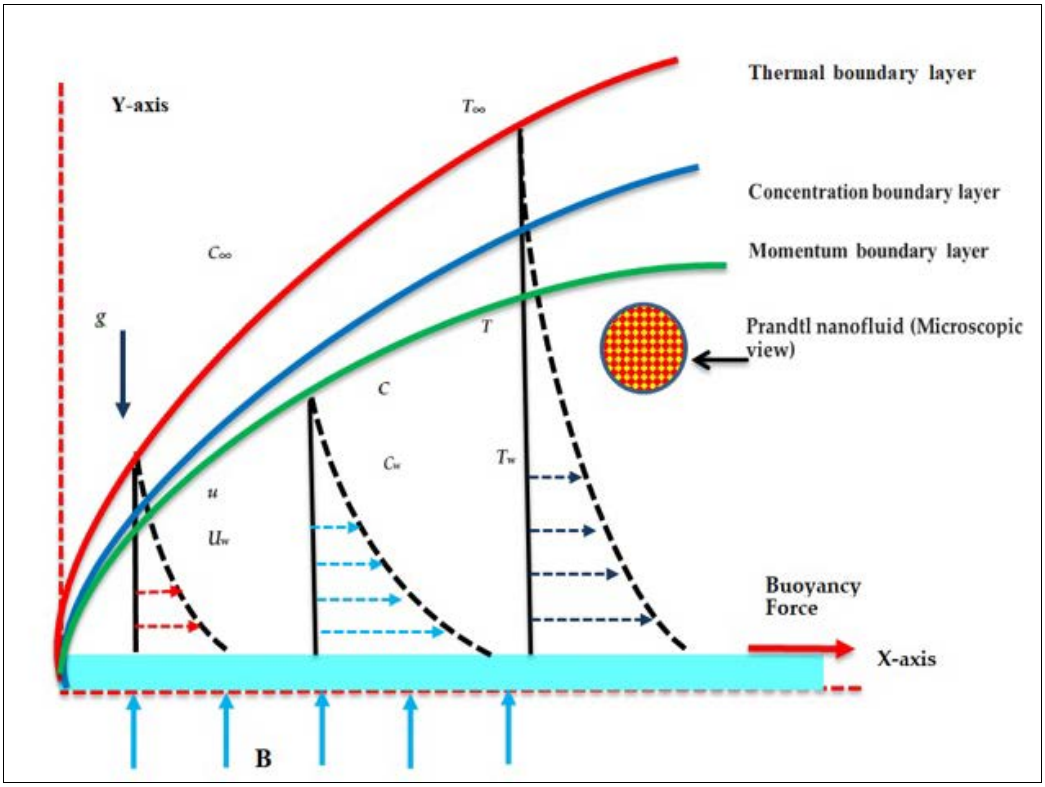

Fig 1: Model of a Flow System

The following are the mathematical formulas with the flow scenario under discussion:

$$\frac{\partial u}{\partial x}+\frac{\partial v}{\partial y}=0 \tag{1}$$

$$\left.\begin{aligned} u\frac{\partial u}{\partial x}+v\frac{\partial u}{\partial y}+\frac{\partial u}{\partial t}=\frac{\partial u_e}{\partial t}+u_e\frac{\partial u_e}{\partial x}+\frac{A}{\rho c_1}\frac{\partial^2 u}{\partial y^2}+\frac{A}{2\rho c_1^3}\left(\frac{\partial u}{\partial y}\right)^2\frac{\partial^2 u}{\partial y^2}-\frac{\sigma B^2 u}{\rho} \\ -\frac{\upsilon}{k}u+g\beta\left(T-T_\infty\right)+g\beta^*(\mathrm{C}-\mathrm{C}_\infty) \end{aligned}\right\} \tag{2}$$

$$u\frac{\partial T}{\partial x}+v\frac{\partial T}{\partial y}+\frac{\partial T}{\partial t}=\frac{k}{\rho c_p}\frac{\partial^2 T}{\partial y^2}-\frac{1}{\rho c_p}\frac{\partial q_r}{\partial y}+\frac{D_m\, k_t}{c_s c_p}\frac{\partial^2 C}{\partial y^2}+\frac{A}{\rho c_1 c_p}\left(\frac{\partial u}{\partial y}\right)^2+\frac{\sigma B^2 u^2}{\rho c_p} \tag{3}$$

$$u\frac{\partial C}{\partial x}+v\frac{\partial C}{\partial y}+\frac{\partial C}{\partial t}=D_m\frac{\partial^2 C}{\partial y^2}+\frac{D_m\,k_t}{T_m}\frac{\partial^2 T}{\partial y^2}+k_r\left(C-C_\infty\right) \tag{4}$$

Boundary conditions:

$$\left.\begin{array}{l} At\ y=0;\ \ u=u_w(x)=\dfrac{ax}{1-ct},\ \ v=0,\ \ T=T_w,\ C=C_w \\ At\ y\to\infty;u\to u_e,\ \ \ T\to T_\infty,\ \ C\to C_\infty \end{array}\right\} \tag{5}$$

One way to express the radiative heat flow q_r is as follows:

$$q_r=-\left(\frac{4\sigma^*}{3k^*}\right)\frac{\partial T^4}{\partial y}.$$

The radiative heat flow following Taylor's expansion of $T^4\cong 4T_\infty^3T-3T_\infty^4$ around T_∞ and which omits higher-value terms, is

$$\frac{\partial q_r}{\partial y}=-\left(\frac{16\sigma^*T_\infty^3}{3k^*}\right)\frac{\partial^2 T}{\partial y^2} \tag{6}$$

Equation (3) in its modified form is expressed as:

$$\left.\begin{array}{l} u\dfrac{\partial T}{\partial x}+v\dfrac{\partial T}{\partial y}+\dfrac{\partial T}{\partial t}=\left(\dfrac{k}{\rho c_p}\right)\dfrac{\partial^2 T}{\partial y^2}+\left(\dfrac{16\sigma^*T_\infty^3}{3k^*\rho c_p}\right)\dfrac{\partial^2 T}{\partial y^2}+\dfrac{D_m\,k_t}{c_s c_p}\dfrac{\partial^2 C}{\partial y^2} \\ \qquad +\dfrac{A}{\rho c_1 c_p}\left(\dfrac{\partial u}{\partial y}\right)^2+\dfrac{\sigma B^2u^2}{\rho c_p} \end{array}\right\} \tag{7}$$

Employing the following similarity invariants;

$$\left.\begin{array}{l} u=\left(\dfrac{ax}{1-ct}\right)f'(\eta),\quad v=-\left(\sqrt{\dfrac{\upsilon a}{1-ct}}\right)f(\eta),\quad \eta=\left(\sqrt{\dfrac{a}{\upsilon(1-ct)}}\right)y, \\ T=T_\infty+(T_w-T_\infty)\theta(\eta),\quad ,\quad u_e=\dfrac{bx}{1-ct}, \\ C=C_\infty+(C_w-C_\infty)\phi(\eta),\qquad u_w=\dfrac{ax}{1-ct}. \end{array}\right\} \tag{8}$$

Applying (12) to equation (5-11) yielded the following non-linear system of equations:

$$\left.\begin{array}{l} \varepsilon\left(f'''+\delta(f'')^2f'''\right)-\lambda(\frac{\eta}{2}f''+f')+ff''-(f')^2+\left(B'\lambda+B'^2\right) \\ -\left(M+K_p\right)f'+Gr\theta+Gm\phi=0 \end{array}\right\} \tag{9}$$

$$\left(1+\frac{4}{3}R\right)\theta''+\Pr\left[f\theta'-\lambda\frac{\eta}{2}\theta'+Du\phi''+Ec\left(\varepsilon(f'')^2+M(f')^2\right)\right]=0 \tag{10}$$

$$\phi"+Sc\left[f\phi'-\lambda\frac{\eta}{2}\phi'+Sr\theta''+G\phi\right]=0 \tag{11}$$

Along with extremes;

$$f(0)=0,\quad f'(0)=1,\quad \theta(0)=1,\quad \phi(0)=1 \tag{12}$$

$$f'(\infty)\to B',\quad \theta(\infty)\to 0,\quad \phi(\infty)\to 0 \tag{13}$$

Quantities like Skin friction $\left(C_f\right)$, Local Sherwood number $\left(Sh_x\right)$, and Local Nusselt number $\left(Nu_x\right)$ have dimensionless representations that are

$$C_f=\frac{\tau_w}{\rho u_w^2(x)},\ Nu_x=\frac{xq_w}{k\left(T_w-T_\infty\right)},\ Sh_x=\frac{xq_m}{D_m\left(C_w-C_\infty\right)} \tag{14}$$

$$\tau_w=\left[\frac{A}{\rho c_1}\frac{\partial u}{\partial y}+\frac{A}{6\rho c_1{}^3}\left(\frac{\partial u}{\partial y}\right)^3\right]_{y=0},q_w=\left(k\frac{\partial T}{\partial y}\right)_{y=0},q_m=\left(D_m\frac{\partial C}{\partial y}\right)_{y=0} \tag{15}$$

Therefore, the engineering quantities that have been changed look like this:

$$\begin{aligned}C_f\,\mathrm{Re}^{1/2}&=\left(\varepsilon f''(0)+\varepsilon\frac{\delta}{3}f''(0)^3\right)\\ Nu_x/\mathrm{Re}^{1/2}&=-\theta'(0)\\ Sh_x/\mathrm{Re}^{1/2}&=-\phi'(0)\end{aligned} \tag{16}$$

Where the local Reynolds number is $\mathrm{Re}_x=ax^2/\upsilon(1-ct)$

3. Numerical Procedure

A shooting strategy is used to evaluate (9-11) and extremes (12-13). Equations (9-11) were transformed into linear equations by introducing variables Y_1,Y_2,Y_3,Y_4,Y_5,Y_6 and Y_7 in order to turn them into an initial value problem.

$$f=Y_1,\quad \frac{df}{d\eta}=Y_2,\quad \frac{d^2f}{d\eta^2}=Y_3,\quad \theta=Y_4,\quad \frac{d\theta}{d\eta}=Y_5,\quad \phi=Y_6,\quad \frac{d\phi}{d\eta}=Y_7 \tag{17}$$

Additionally defined are the following:

$$\left.\begin{aligned}&f'(\eta)=F_1,\ f''(\eta)=F_2,\ f'''(\eta)=F_3,\\ &\theta'(\eta)=F_4,\ \theta''(\eta)=F_5,\ \phi'(\eta)=F_6,\ \phi''(\eta)=F_7\end{aligned}\right\} \tag{18}$$

The following system of equations is produced by substituting the aforementioned parameter in equations (9) through (17).

$$F_1=Y_2$$

$$F_2=Y_3$$

$$F_3=\frac{\lambda\left(\frac{\eta}{2}Y_3+Y_2\right)+\left(Y_2\right)^2-Y_1Y_3-\left[B'\lambda+\left(B'\right)^2\right]-\left(GrY_4+GmY_6\right)+\left(M+Kp\right)Y_2}{\varepsilon+\varepsilon\delta\left(Y_3\right)^2} \tag{19}$$

$$F_4 = Y_5,$$

$$F_5 = \frac{3\,\mathrm{Pr}}{3+4R-3\,\mathrm{PrDuScSr}}\left[\begin{array}{l} Y_5\left(\frac{\eta}{2}\lambda - Y_1 + GY_6\right) - \varepsilon Ec\left(Y_3\right)^2 - EcM\left(Y_2\right)^2 \\ -DuSc\left(\frac{\eta}{2}\lambda - Y_1 + GY_6\right)Y_7 \end{array}\right] \tag{20}$$

$$F_6 = Y_7,$$

$$F_7 = \frac{3ScSr\,\mathrm{Pr}\left[\left(\frac{\eta}{2}\lambda - Y_1 + GY_6\right)Y_5 - \varepsilon Ec\left(Y_3\right)^2 - EcM\left(Y_2\right)^2\right] - \left(3+4R\right)ScY_7\left(\frac{\eta}{2}\lambda - Y_1 + GY_6\right)}{3ScSr\,\mathrm{Pr}\,Du - 3 - 4R} \tag{21}$$

with the extreme conditions,

$$\left.\begin{array}{l} \text{At } \eta \to 0; \quad Y_1(\eta) = 0,\ Y_2(\eta) = 1,\ Y_4(\eta) = 1,\ Y_6(\eta) = 1 \\ \text{At } \eta \to \infty; \quad Y_2\left(\eta\right) = B', Y_4(\eta) = 0,\ \ Y_6(\eta) = 0 \end{array}\right\} \tag{22}$$

Both the first order translated equation (19) to (21) and the reduced reference starting condition of equation (22) are solved.

Results analysis

Graphs representing the heat and mass (θ, ϕ) distributions as well as the numerical findings of an unstable incompressible Prandtl fluid flowing across a stretched sheet have been shown. It has been thoroughly examined the fluid term (ε) influence the temperature and velocity distributions in the Prandtl fluid flow. The parameter (ε) is closely related to the fluid's rheological characteristics, potentially representing a non-dimensional form of thermal conductivity or internal fluid resistance. With different fluid parameter values, the velocity distribution versus stream term (η) is shown in Figure 2. As ε increases, the velocity profile exhibits a distinct decrease, particularly near the surface of the porous stretching device.

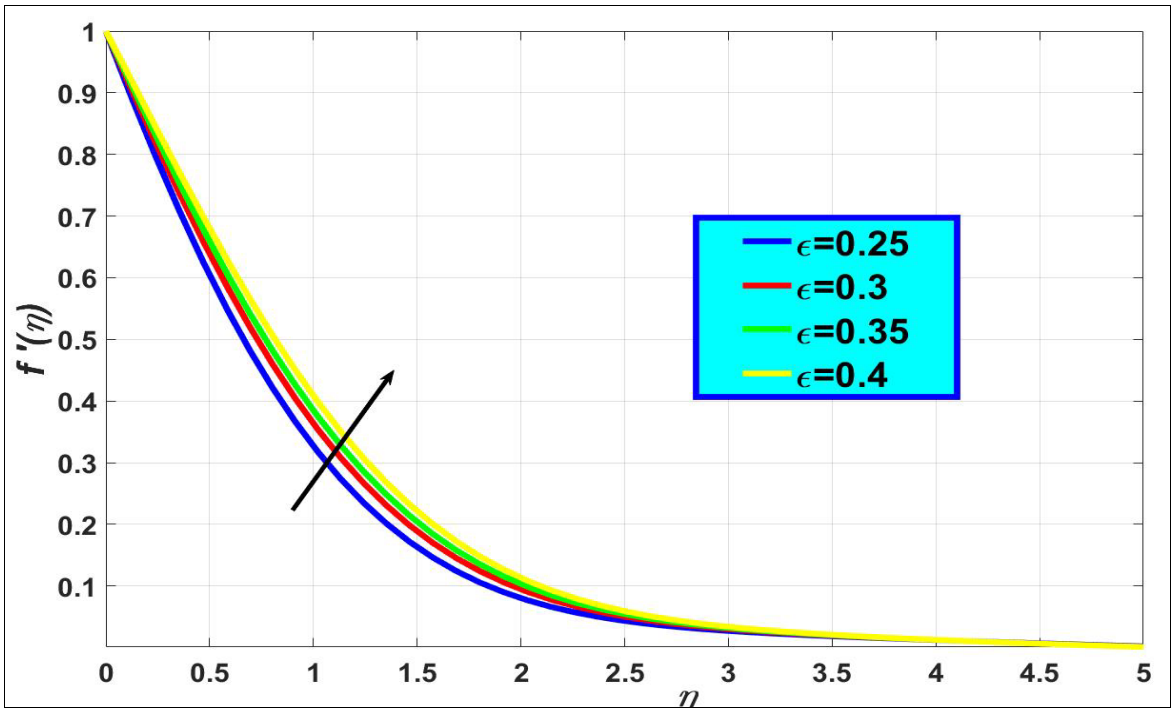

Fig 2: Effect of ε on $f'(\eta)$

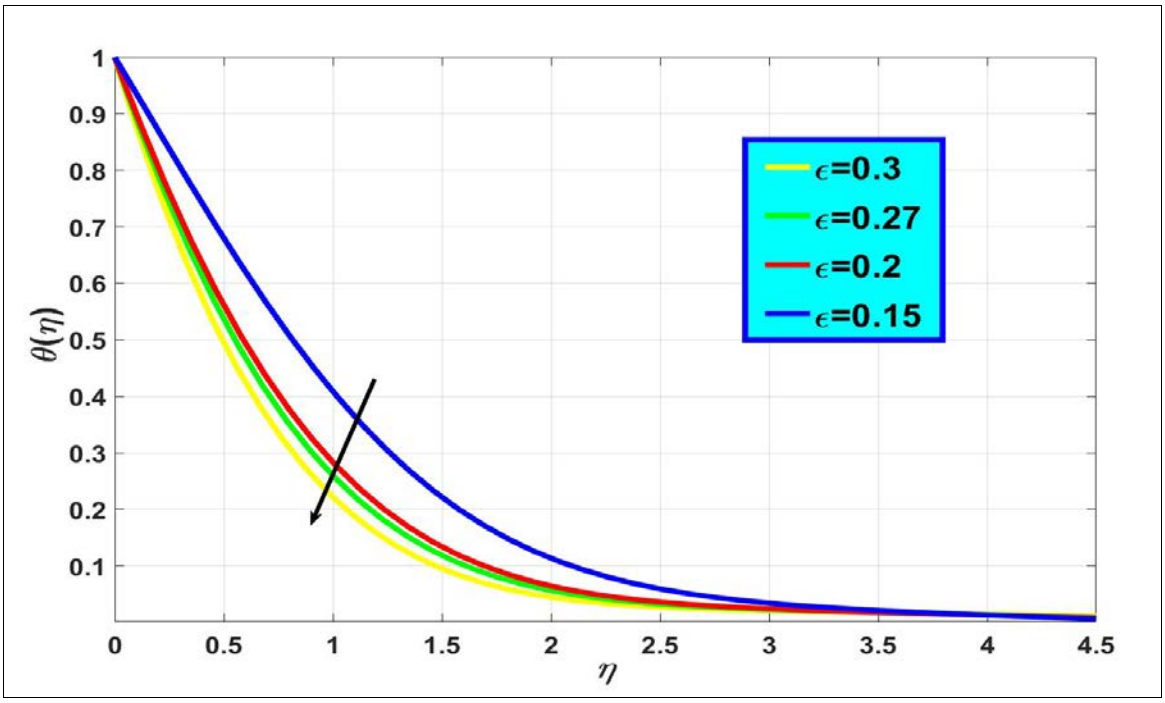

Fig 3: Effect of ε on $\theta(\eta)$

Figure 4 illustrates how the magnetic field (M) affects the velocity. As the strength of the magnetic field increases, the velocity noticeably decreases.

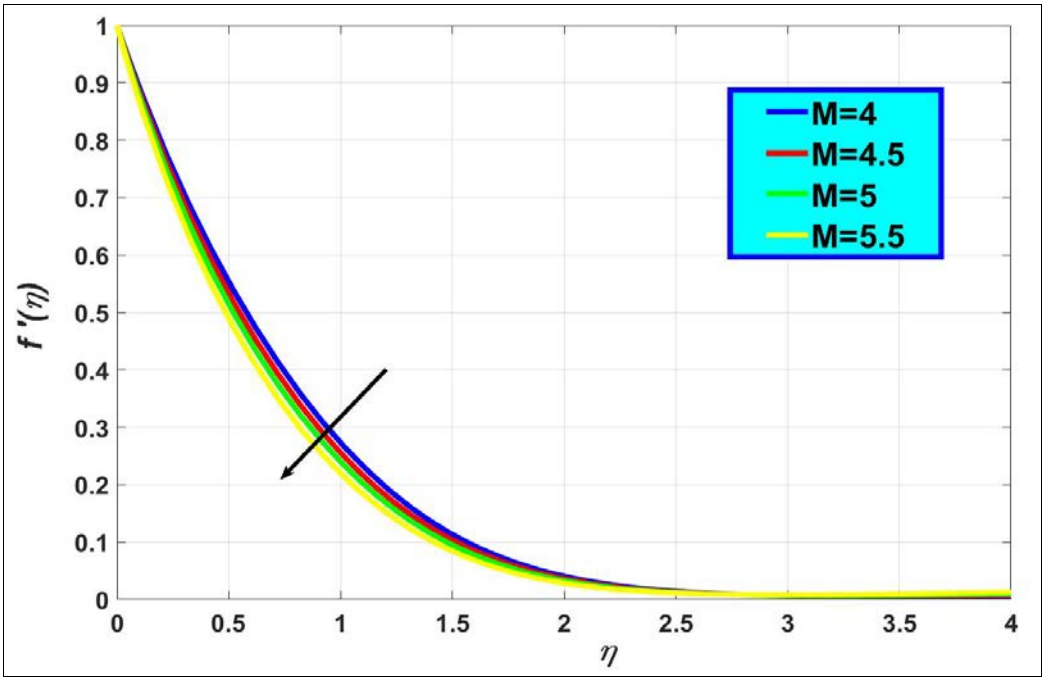

Fig 4: Effect of M on $f'(\eta)$

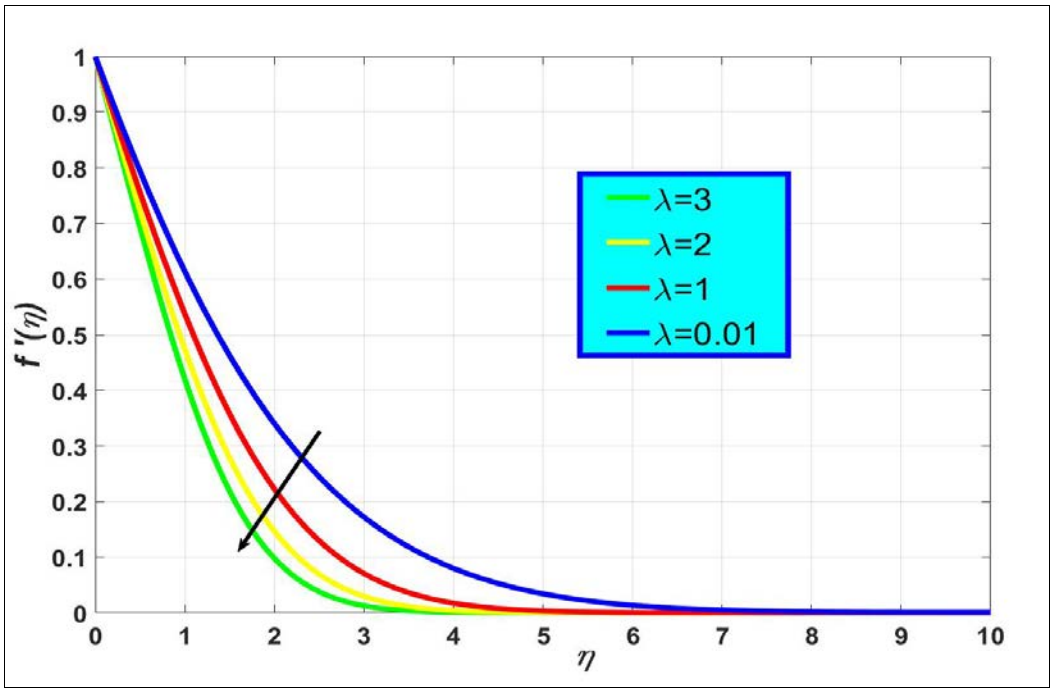

Fig 5: Influence of (λ) on $f'(\eta)$

Figure 5 illustrates the impact of the unstable parameter on fluid motion. The λ typically represents the time-dependent effects on the fluid's motion. When the λ increases, the velocity profile exhibits time-dependent fluctuations**.** For greater values of the (λ), the flow experiences delayed acceleration **or** slower deceleration**,** depending on the nature of the transient forces acting on the system.

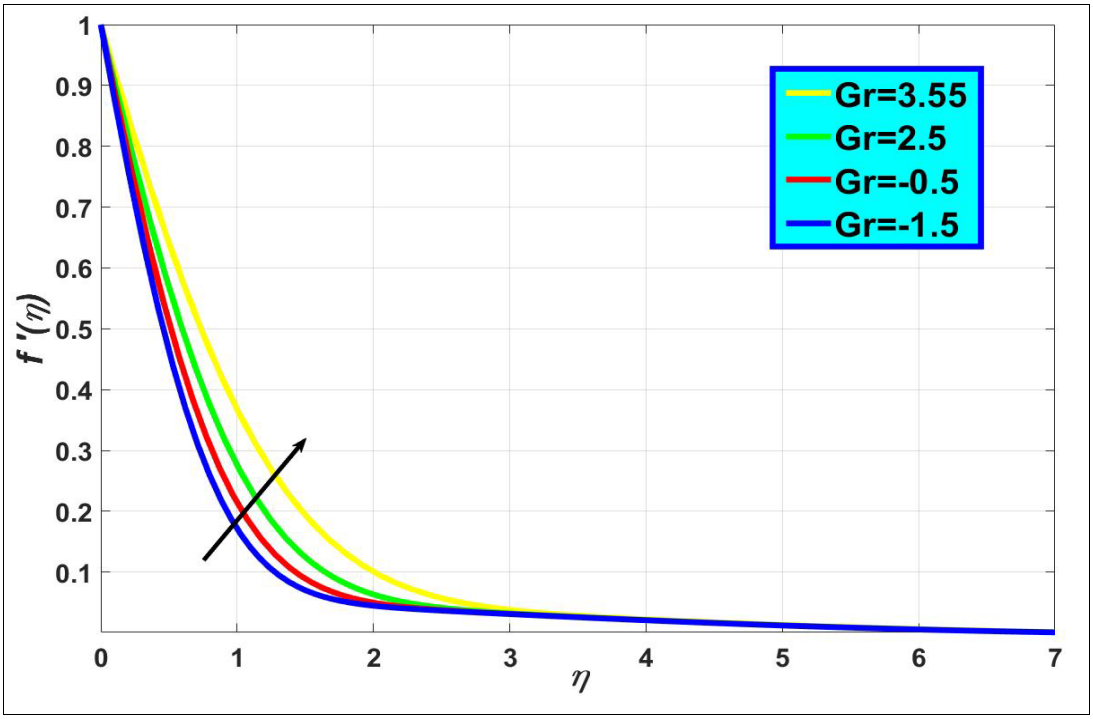

Fig 6: Effect of Gr **on** $f'(\eta)$

The velocity performance regarding Grashof number (Gr) is seen in Figure 6. The Gr is an important dimensionless parameter that quantifies the influence of buoyancy forces (due to concentration gradients) on the fluid flow. A hike in the Gr leads to a greater influence of buoyancy forces on the flow. As Gr increases, the velocity near the surface increases due to the enhanced buoyant forces**,** which help drive the fluid motion.

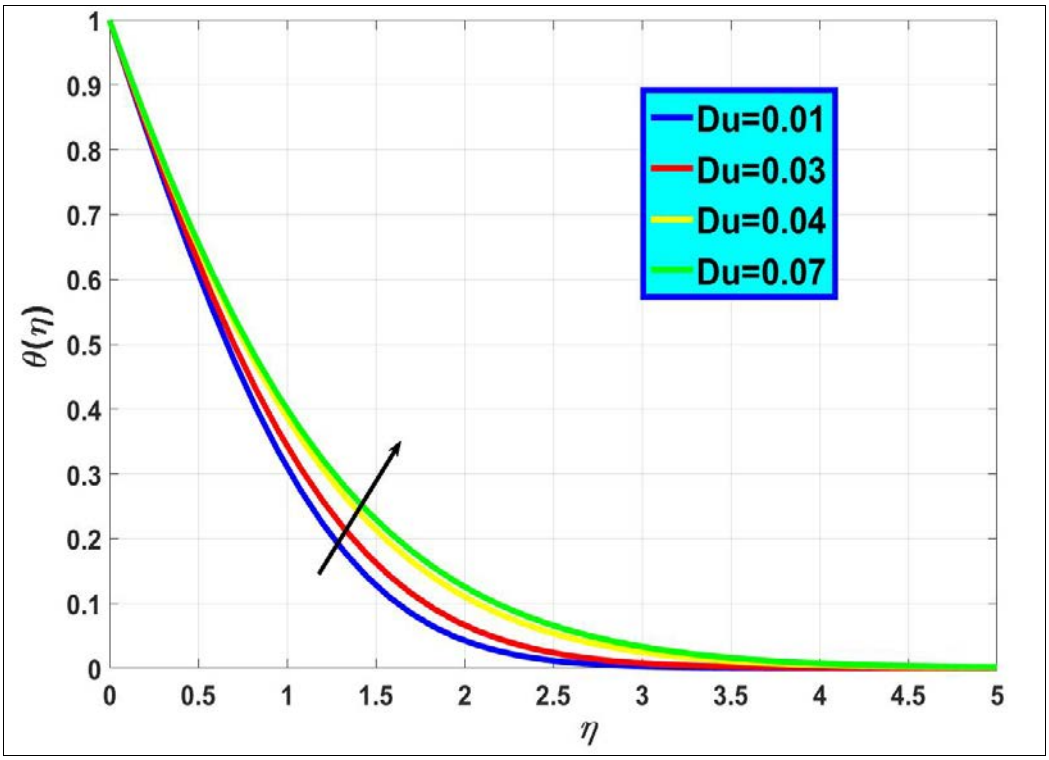

Fig 7: Effect of Du on $\theta(\eta)$

Figure 7 illustrates the $\theta(\eta)$ is affected by the Dufour number (Du). The Du is a dimensionless number that characterizes the coupled effects of double diffusion in a fluid. As the Du escalate, the thermal diffusion effect becomes more significant**,** leading to changes in the temperature profile.

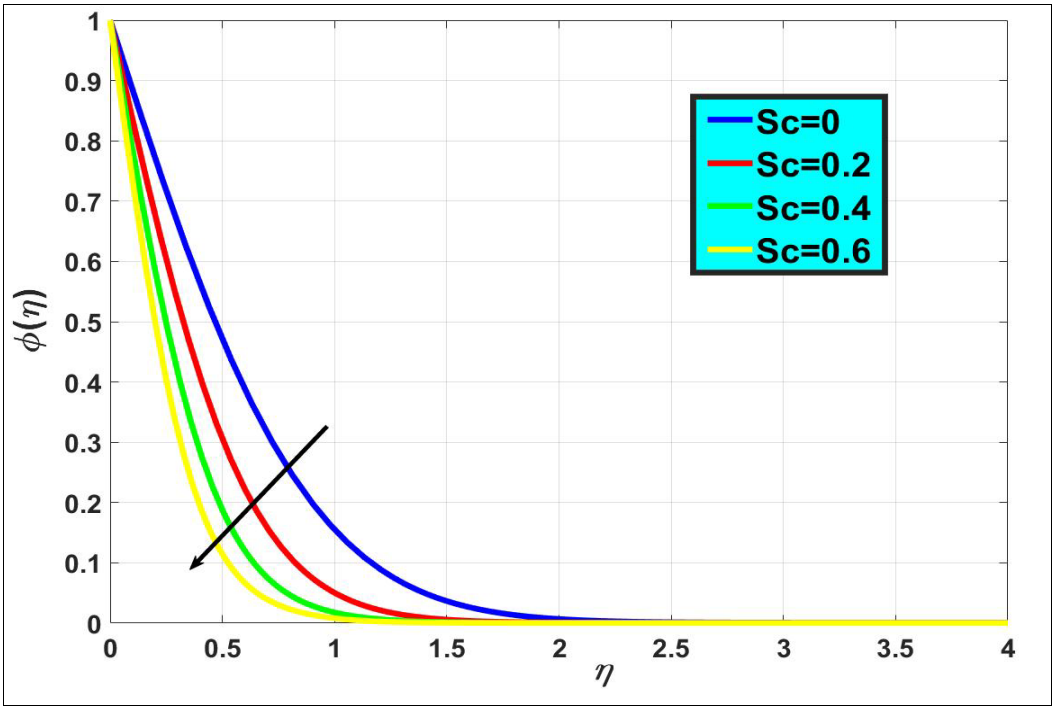

Fig 8: Effect of Sc on $\phi(\eta)$

Figure 8 illustrates influence of Sc on $\phi(\eta)$. The fluid's mass diffusion and momentum diffusion are characterized by their relative significance. The Sc has a significant effect on the concentration distribution in fluid flows, particularly in the presence of concentration gradients, such as in diffusion or chemical reaction processes. As the Sc increases, the diffusivity of the solute decreases relative to the fluid's viscosity. Figure 11 shows how the permeability of the medium (Kp) affects fluid velocity. When the permeability increases, the medium offers less
resistance to the flow, allowing the fluid to move more freely through the porous matrix.

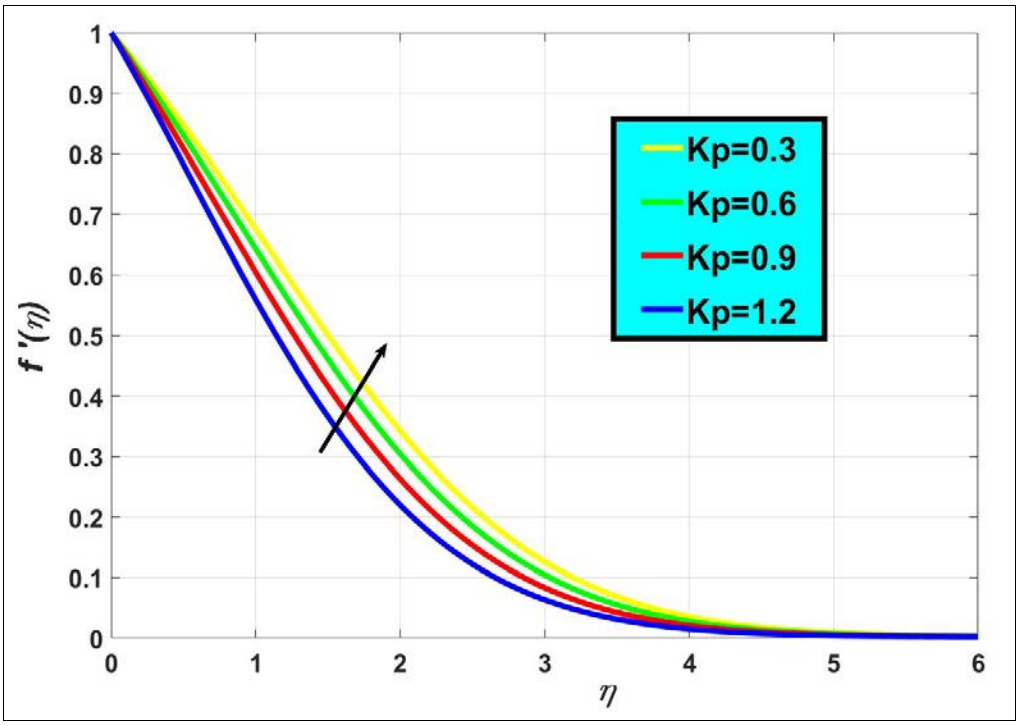

Fig 9: Effect of Kp on $f'(\eta)$

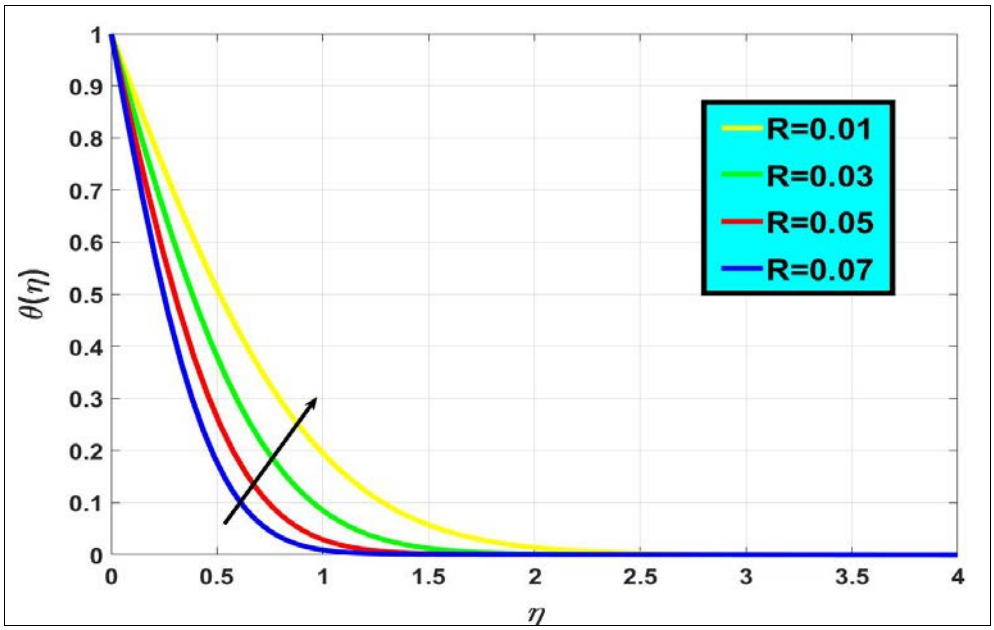

Figure 10: Effect of R on $\theta(\eta)$

Figure 10 illustrates how fluid temperature is affected by thermal radiation (R). The analysis reveals that an increase in the radiation parameter leads to a significant enhancement in the fluid temperature throughout the boundary layer.

5. Conclusion

This study thoroughly examined the combined effects of thermal radiation, chemical reactions, and resistive (Joule) heating on heat and mass transfer in Prandtl fluids. The results show that thermal radiation greatly improves the temperature distribution, while chemical reactions affect the concentration profiles. Additionally, resistive heating causes a significant increase in the fluid temperature. The interaction of these mechanisms changes the thermal and solutal boundary layers, with radiation boosting thermal diffusion and chemical reactions altering mass transport properties. Overall, the combined effects of these processes are essential for optimizing thermal systems that use Prandtl fluids, such as energy devices, polymer processing, and chemical reactors.

Nomenclature

- a, b, c Stretching constants [1/s]
- A Consistency coefficient
- B' Upstream velocity [m/s]

- B_0 Uniform magnetic field [T]
- c_1 Material fluid parameter
- C Species concentration [kg/m^2]
- C_w Surface concentration
- C_∞ Ambient concentration [mol/m^3]
- C_f Friction drag
- C_p Latent heat [J/Kg K]
- D_m Mass diffusivity
- Du Dufour number
- D_T Thermophoresis coefficient [m^2/s]
- Ec Eckert number
- g Acceleration due gravity [m/s^{-2}]
- G Chemical Reaction Parameter
- Gr Thermal Grashof number
- Gm Solutal Grashof number
- k Thermal conductivity [Wm^{-1}K^{-1}]
- k^* Mean absorption coefficient
- k_r Coefficient of chemical reaction
- M Magnetic parameter
- Nu_x Local Nusselt number
- Pr Prandtl number
- q_r Radiative heat flux [W/m^2]
- q_m Mass flux
- R Thermal radiation parameter
- Re_x Local Reynolds number
- Sc Schmidt number
- Sr Soret number
- Sh_x Local Sherwood number
- t Time [s]
- T Fluid temperature [K]
- T_w Temperature at the wall [K]
- T_∞ Ambient temperature [K]
- u, v Velocity components [m/s]
- u_w Stretching velocity [m/s]

Greek symbols

- ε, δ Prandtl fluid parameter
- ρ Fluid density [kg/m^3]
- ρc_p Thermal capacity [Jkg^{-1}K^{-1}]
- σ^* Stefan's constant [Wm^{-2}K^{-4}]
- η Similarity invariants
- θ Relative temperature
- ϕ Relative concentration
- ν Momentum diffusivity [m^2/s]
- τ_{xy} Stress-strain tensor
- μ Coefficient of viscosity [kg/m s]

Subscripts

- w Amount at wall
- ∞ Distance from the sheet

Reference

1. Farrokhi H, Otuya DO, Khimchenko A, Dong J. Magnetohydrodynamics in biomedical applications. In: Nanofluid Flow in Porous Media. London: IntechOpen; 2019. p. 1-26.
2. Ali F, Ali F, Sheikh NA, Khan I, Nisar KS. Caputo-Fabrizio fractional derivatives modeling of transient MHD Brinkman nanoliquid: applications in food technology. Chaos Solitons Fractals. 2020;131:109489.
3. Rajput GR, Patil VS, Jadhav BP. MHD mixed flow of unsteady convection with radiation over a vertical porous plate: Lie group symmetry analysis. Applied and Computational Mechanics. 2017;11(2):1-12. Available from: http://hdl.handle.net/11025/26592
4. Amanulla CH, Saleem S, Wakif A, AlQarni MM. MHD Prandtl fluid flow past an isothermal permeable sphere with slip effects. Case Studies in Thermal Engineering. 2019;14:100447. Available from: https://doi.org/10.1016/j.csite.2019.100447
5. Hussain A, Malik MY, Awais M, Salahuddin T, Bilal S. Computational and physical aspects of MHD Prandtl-Eyring fluid flow analysis over a stretching sheet. Neural Computing and Applications. 2019;31(1):425-33. Available from: https://doi.org/10.1007/s00521-017-3017-5
6. Hayat T, Asghar S, Tanveer A, Alsaedi A. Homogeneous-heterogeneous reactions in peristaltic flow of Prandtl fluid with thermal radiation. Journal of Molecular Liquids. 2017;240:504-513.
7. Rajesh R, Rajasekhara Gowd Y. Heat and mass transfer analysis on MHD peristaltic Prandtl fluid model through a tapered channel with thermal radiation. Journal of Applied and Computational Mechanics. 2019;5(5):951-963. Available from: https://dx.doi.org/10.22055/jacm.2019.27998.1450
8. Patil VS, Patil AB, Ganesh S, Humane PP, Patil NS. Unsteady MHD flow of a nano Powell-Eyring fluid near stagnation point past a convectively heated stretching sheet in the existence of chemical reaction with thermal radiation. Materials Today: Proceedings. 2021;44:3767-76. Available from: https://doi.org/10.1016/j.matpr.2020.11.860
9. Sivasankaran S, Bhuvaneswari M, Alzahrani AK. Numerical simulation on convection of non-Newtonian fluid in a porous enclosure with non-uniform heating and thermal radiation. Alexandria Engineering Journal. 2020;59(5):3315-3323.
10. Nayak MK, Pandey VS, Shaw S, Makinde OD, Ramadan KM, Henda MB, Tlili I. Thermo-fluidic significance of non-Newtonian fluid with hybrid nanostructures. Case Studies in Thermal Engineering. 2021;26:101092.
11. Khan Z, Khan I, Ullah M, Tlili I. Effect of thermal radiation and chemical reaction on non-Newtonian fluid through a vertically stretching porous plate with uniform suction. Results in Physics. 2018;9:1086-1095.
12. Patil AB, Humane PP, Patil VS, Rajput GR. MHD Prandtl nanofluid flow due to convectively heated stretching sheet below the control of chemical reaction with thermal radiation. International Journal of Ambient Energy. 2021;24:1-13.
13. Patil AB, Patil VS, Humane PP, Shamshuddin MD, Jadhav MA. Double diffusive time-dependent MHD Prandtl nanofluid flow due to linear stretching sheet with convective boundary conditions. International Journal of Modelling and Simulation. 2022;1-15. Available from: https://doi.org/10.1080/02286203.2022.2033499
14. Hayat T, Zahir H, Tanveer A, Alsaedi A. Soret and Dufour effects on MHD peristaltic flow of Prandtl fluid in a rotating channel. Results in Physics. 2018;8:1291-300. Available from: https://doi.org/10.1016/j.rinp.2018.01.058
15. Batool S, Siddiqui BK, Malik MY, Alqahtani AS, ul Hassan QM. Double diffusion in stretched flow over a stretching cylinder with activation energy and entropy generation. Case Studies in Thermal Engineering. 2021;26:101119. Available from: https://doi.org/10.1016/j.csite.2021.101119
16. Rauf A, Shehzad SA, Abbas Z, Hayat T. Unsteady three-dimensional MHD flow of the micropolar fluid over an oscillatory disk with Cattaneo-Christov double diffusion. Applied Mathematics and Mechanics. 2019;40(10):1471-86.
17. Hafeez A, Khan M, Ahmed A, Ahmed J. Rotational flow of Oldroyd-B nanofluid subject to Cattaneo-Christov double diffusion theory. Applied Mathematics and Mechanics. 2020;41:1083-1094.
18. Waqas H, Manzoor U, Muhammad T, Hussain S. Thermo-bioconvection transport of nanofluid over an inclined stretching cylinder with Cattaneo-Christov double-diffusion. Communications in Theoretical Physics. 2021;73(7):075006. Available from: https://doi.org/10.1088/1572-9494/abfcb9
19. Mishra A, Kumar M. Velocity and thermal slip effects on MHD nanofluid flow past a stretching cylinder with viscous dissipation and Joule heating. SN Applied Sciences. 2020;2(8):1-13.
20. Jawad M, Saeed A, Bilal M, Gul T, Khan A, Nasir S. The impact of magnetohydrodynamic on bioconvection nanofluid flow with viscous dissipation and Joule heating effects. Engineering Research Express. 2021;3(1):015030.
21. Shamshuddin MD, Narayana PS. Combined effect of viscous dissipation and Joule heating on MHD flow past a Riga plate with Cattaneo-Christov heat flux. Indian Journal of Physics. 2020;94(9):1385-1394.
22. Ahmed F, Iqbal M, Akbar NS. Viscous dissipation and joule heating effects on forced convection power law fluid flow through annular duct. Proceedings of the Institution of Mechanical Engineers, Part C: Journal of Mechanical Engineering Science. 2021;235(21):5858-5865.
23. Swain BK, Parida BC, Kar S, Senapati N. Viscous dissipation and joule heating effect on MHD flow and heat transfer past a stretching sheet embedded in a porous medium. Heliyon. 2020;6(10):e05338. Available from: https://doi.org/10.1016/j.heliyon.2020.e05338
24. Patil AB, Patil NS, Patil VS, Humane PP, Rajput GR. Unsteady thermally radiative Prandtl fluid flow past a magnetized inclined porous stretching device with double-diffusion, viscous dissipation, and Joule heating. Proceedings of the Institution of Mechanical Engineers, Part E: Journal of Process Mechanical Engineering. 2023;237(3):762-70. Available from: https://doi.org/10.1177/09544089221107295